atom were responsible for the change, then the data for x(Pb) = 0.3 and 0.7 samples should be the same.
27. J. Ren *et al.*, *Physica C* **158**, 501 (1989); L. F. Mattheiss and D. R. Hamann, *Phys. Rev. B* **38**, 5012 (1988).
28. We acknowledge helpful discussions with D. S. Ginley, E. L. Venturini, B. Morosin, and R. J. Baughman, and we thank Y. J. Uemura, G. M. Luke, and B. J. Sternlieb for assistance with the magnetic measurements. This work was supported by the David and Lucile Packard Foundation, the National Science Foundation, and Rohm and Haas.

17 January 1990; accepted 27 March 1990

Explosive Deep Water Basalt in the Sumisu Backarc Rift

J. Gill, P. Torssander, H. Lapierre, R. Taylor, K. Kaiho, M. Koyama, M. Kusakabe, J. Aitchison, S. Cisowski, K. Dadey, K. Fujioka, A. Klaus, M. Lovell, K. Marsaglia, P. Pezard, B. Taylor, K. Tazaki

Eruption of 1-million-year-old tholeiitic basalt >1800 meters below sea level (>18 megapascals) in a backarc rift behind the Bonin arc produced a scoriaceous breccia similar in some respects to that formed during subaerial eruptions. Explosion of the magma is thought to have produced frothy agglutinate which welded either on the sea floor or in a submarine eruption column. The resulting 135-meter-thick pyroclastic deposit has paleomagnetic inclinations that are random at a scale of <2.5 meters. High magmatic water content, which is about 1.3 percent by weight after vesiculation, contributed to the explosivity.

Deep water explosive volcanism is an unwitnessed phenomenon that frequently is appealed to as an explanation of marine volcaniclastic rocks (*1*). Unlike subaerial volcanoes, submarine ones vent to pressure greater than atmospheric and erupt into a medium that has higher density, heat capacity, and conductivity than air. Consequently, higher magmatic gas contents are necessary for internally driven explosions, exsolved gas differs in composition, clasts quench faster, and eruption dynamics differ. This contrast also applies to volcanism into denser atmospheres on other planetary bodies such as Venus.

Before magma explodes it vesiculates. Tholeiitic basalt lavas with more than 10% vesicles by volume generally erupt in water shallower than 500 to 800 m below sea level (mbsl) and outgas mostly CO_2 (*2*). More highly vesicular tholeiite lavas associated with deep water sediments are most common in backarc basins (*3*). Submarine pyroclastic rocks are also common in the geologic record but most are sufficiently old that their geologic setting at the time of eruption is uncertain and their volcanologically diagnostic characteristics have degraded. There is disagreement whether the responsible explosions occurred in deep water (*1*) and were internally or externally driven. Explosivity due to exsolution of magmatic gas is thought to require gas/melt ratios of about 3 (*4*), whereas externally driven steam explosivity merely requires vigorous dynamic contact between magma and water (*5*). The maximum pressure for either kind of explosivity is unknown, but has been thought to be 10 to 30 MPa (*6*). In this report we describe a late Pleistocene scoriaceous tholeiitic basalt breccia that apparently erupted explosively at >1800 mbsl (18 MPa) during the initial rifting stage of a backarc basin. Eruption resulted in thorough fragmentation of the magma into frothy shards that then welded into agglutinate in the eruption column or on the sea floor. Consequently, all the traits described below that conventionally are associated with subaerial eruption—high vesicularity, explosivity, hot deposition, and thin cooling units—also can form at moderate pressure, for example, in deep water.

The breccia was discovered at Site 791 of

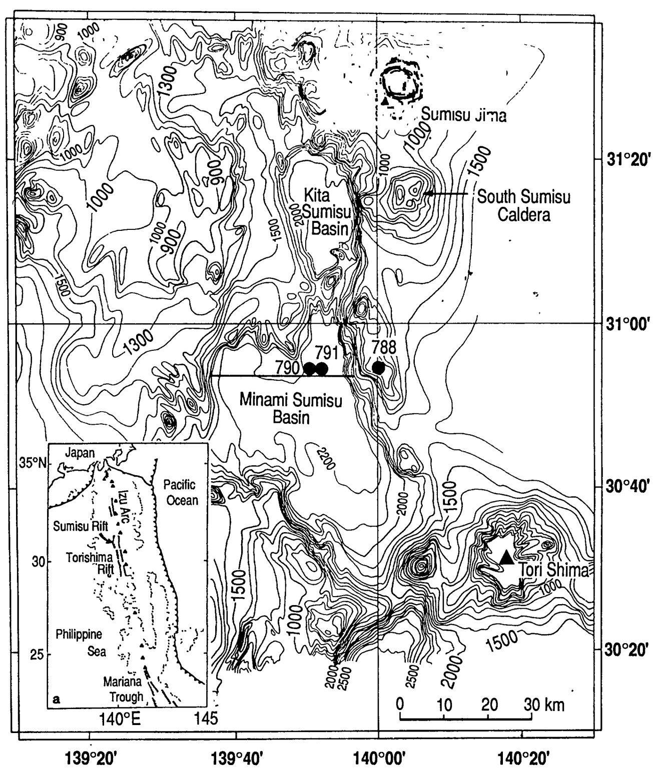

Fig. 1. Location map. Sites 788, 790, and 791 were drilled during ODP Leg 126. The volcanic arc extends from Sumisu Jima through Site 788 to Tori Shima. Kita and Minami Sumisu basins constitute the Sumisu Rift, the location of which is shown in the inset.

J. Gill, Earth Sciences Board and Institute of Marine Studies, University of California, Santa Cruz, CA 95060, USA.
P. Torssander, Department of Geology, University of Stockholm, S-106 91, Stockholm, Sweden.
H. Lapierre, Laboratoire de Geologie Structurale, Universite d'Orleans, 45067 Orleans Cedex 2 France.
R. Taylor, Department of Geology, University of Southampton, Hampshire S09 5NH England.
K. Kaiho, Institute of Geology and Paleontology, Tohoku University, Sendai 980 Japan.
M. Koyama, Institute of Geosciences, Shizuoka University, Shizuoka 422 Japan.
M. Kusakabe, Institute for Study of Earth's Interior, Okayama University, Misasa, Tottori-ken 682-02 Japan.
J. Aitchison, Department of Geology and Geophysics, University of New England, Armidale, NSW, Australia, 2351.
S. Cisowski, Department of Geological Sciences, University of California, Santa Barbara, CA 93106.
K. Dadey, Graduate School of Oceanography, University of Rhode Island, Kingston, RI 02811.
K. Fujioka, Ocean Research Institute, University of Tokyo, 1-15-1 Nakano, Tokyo 164 Japan.
A. Klaus and B. Taylor, Hawaii Institute of Geophysics, University of Hawaii, Honolulu, HI 96822.
M. Lovell, Geology Department, Leiscester University, Leicester LE1, 7RH England.
K. Marsaglia, Department of Geology, University of Texas, El Paso, TX 79968.
P. Pezard, Lamont-Dohert Geological Observatory, Palisades, NY 10964.
K. Tazaki, Department of Geology, Shimane University, Matsue, Japan.

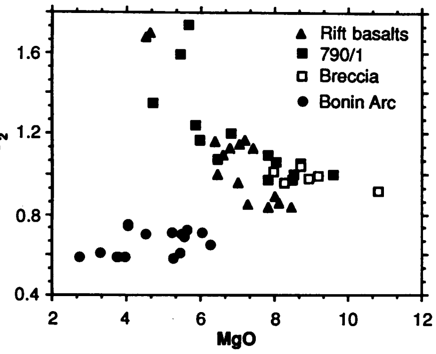

Fig. 2. MgO versus TiO_2 for basalts from Sites 790 and 791, including the breccia. Comparative data for the younger Sumisu Rift sea floor basalts are from (*11*); data for the Bonin Arc are from (*14*) and (*19*).

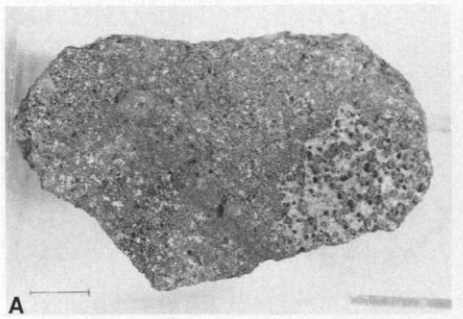

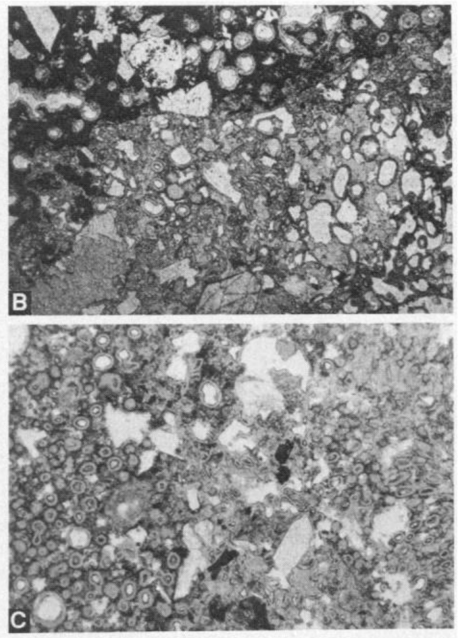

Fig. 3. (**A**) Representative core of breccia, 6.5 cm long. One large clast (2.3 cm in diameter, light gray, with larger vesicles) and several smaller clasts occur within matrix. Scale bar = 1 cm. Sample 791B-68R-1, piece 10. (**B**) Photomicrograph of representative breccia in transmitted light showing the boundary between clast (dark, upper left) and matrix (light, lower right). The euhedral plagioclase phenocrysts of the clast are clearly visible as are its 0.2-mm vesicles lined with 1- to 2-μm-thick smectite. The black groundmass consists of devitrified glass, plagioclase microlites, and submicroscopic crystals. Euhedral plagioclase and olivine crystals are visible in the matrix where the size and linings of vesicles are the same as in the clast. The matrix is lighter in color because its glass is fresh. The contact between matrix and clast exhibits complex 0.05-mm-wide zones of alteration in the lower left and upper right of the figure. Note the broken plagioclase phenocryst of the clast at the contact. Sample 791-B-62R, piece 5b; ×40 magnification; the field of view is 3 mm in the long dimension. (**C**) Photomicrograph of matrix showing an annealed contact between scoriaceous domains, one more plastically deformed than the other. Sample 791B-67R-1, piece 5, for which a complete analysis is given in Table 1. Magnification as in (B).

Ocean Drilling Program (ODP) Leg 126 in the Sumisu Rift, which is forming behind the Izu-Bonin island arc (*7*) (Fig. 1). Quaternary volcanism occurs in the rift and along both the active and remnant arcs that flank it (*8*). The arc volcanoes rise from a ridge about 1200 mbsl; the rift floor is about 2200 mbsl. Site 791 is 5 km west of the master boundary fault of the rift in an east-dipping half-graben. About 1 km of sediment overlies the basaltic basement. The upper half of the sediment is mostly arc-derived clastic material. The lower sediments are nannofossil-rich clays, thin ash beds, and scattered pumice and scoria clasts. The basal sediment was deposited 1.05 to 1.10 million years ago (Ma) (*7*).

The stratigraphy of the cores implies that the volcanic basement was erupted and deposited deeper than 1800 mbsl. Benthic foraminifers in the clay immediately and conformably above the basement (*9*) indicate deep water depths (>2000 mbsl). This inference is based on a comparison with Quaternary foraminifers collected during Leg 126 and offshore of Shikoku, Japan (*10*). Because the rift formed quickly, however, water depth might have been shallower during volcanism than during subsequent sedimentation. Basalts of similar age and composition were collected with ALVIN at 1832 to 2075 mbsl from the adjacent rift wall (*11*). However, as shown below, the volcanic rocks that erupted at shallower depth on the arc are quite different in composition (Fig. 2). Thus, the volcanic rocks forming the basement of Site 791, which is now >3000 mbsl, are thought to have both erupted and accumulated on the rift floor or lower rift wall between 1800 and 2500 mbsl.

About half of the basement at Site 791 is scoriaceous basalt breccia. It forms a stratigraphic unit 135 m thick in which core recovery was 13%. Neither bedding, lamination, or grading, nor pelagic sediment interbeds were recognized in the breccia. The breccia was not recovered in basement cores at Site 790 located only 2.4 km to the west.

Macroscopically the scoriaceous breccia consists of gray clasts up to 6 cm in diameter in a green-gray matrix (Fig. 3A). The clasts and matrix are similar and consist primarily of highly expanded sideromelane. Both are sparsely phyric with 1 to 4% by volume of olivine and plagioclase. The minerals are euhedral, 0.5 to 1.0 mm in diameter, and fresh near the top of the section. Olivines (Fo_{81}) contain spinel inclusions (*12*). Plagioclases have An_{83-87} cores and Ar_{70-80} rims (*12*); some crystals are oscillatorally zoned.

The clasts appear to be monomictic. Their groundmass is intersertal and microvesicular. The vesicles have an average diameter of 0.1 to 0.2 mm and form a honeycomb texture; vesicle walls are 0.05 to 0.2 mm thick. These vesicles are an order of magnitude smaller and more abundant than is typical of mid-ocean ridge basalt (MORB) (*2*). The vesicle volume in the clasts was estimated visually to be 30 to 40%, in agreement with porosities calculated from wet and dry weights for four clasts. This contrasts with estimated vesicularities and calculated porosities of 20 to 30% in overlying lava. The largest glass shards in the matrix lie under these clasts and appear to have broken from them or been annealed to them. Most large clasts have angular and irregular shapes due to burst vesicles, but some exterior vesicle walls as thin as 0.1 mm have remained intact. Some phenocrysts are broken at clast margins (Fig. 3B).

The matrix of the breccia consists of glass and crystals of plagioclase and olivine. Some glass shards are nonvesicular over areas up to 25 mm^2, but most are highly vesicular throughout and have diffuse boundaries. Domains of variably vesiculated and deformed scoria can be recognized, welded together as in subaerial agglutinate (Fig. 3C). The material between crystals and recognizable shards is everywhere microvesicular. The vesicle volume in the matrix was estimated visually to be 40 to 50%. Porosities calculated from wet and dry weights of the matrix are 36 ± 9% (1σ, 16 samples).

Both clasts and matrix become more altered with depth. In the top 30 m, vesicles are open with thin smectite linings. Deeper, smectite also occurs along cracks in olivine, and some vesicles are filled with smectite, calcite, or zeolite (Fig. 3A). Still deeper, all olivine is replaced by iddingsite, calcite, and magnetite. Plagioclase remains fresh throughout the section. Glass becomes more devitrified, but is consistently fresher in the matrix than in the clasts. This difference preserves a color contrast in hand specimen. Vesicles are more consistently flattened in the bottom third of the section.

In order to investigate the cooling history of the breccia, the paleomagnetism of 21 minicores (10 cm^3) of matrix and 6 of clasts was studied. Seven samples were cut into three or four small disks of about 3 cm^3 and measured separately to evaluate the scale of homogeneity. The median destructive fields and mean blocking temperatures ranged from 30 to 46 mT and 300° to 400°C, respectively. Intensities of the matrix were 0.1 to 5 A/m; intensities of the clasts were 7 to 20 A/m. Most specimens have a single component of thermoremanent magnetization, 90% of which was acquired between 300° and 550°C. The remanence directions are stable and changed less than 5° through the stepwise thermal and alternating field demagnetizations. The high intensities and stable remanence, together with the petrographic evidence of welded and plastically deformed volcanic glass, indicate that the remanent magnetization is thermal in origin. Both the clasts and matrix have the rock magnetic properties of subaerial lava.

Both clasts and matrix are mafic tholeiitic basalt (Table 1). Matrix-rich samples typically have higher K_2O and LOI, and lower P_2O_5, Y, and Sr contents than clasts. Both clasts and matrix, together with lavas and diabases from elsewhere in the core, are compositionally distinct from island arc basalts and MORBs (Fig. 2). Chemically as well as geographically, they are backarc basin basalts (*13*). They are broadly similar in composition to basalts from adjacent sea floor outcrops of pillow lava 5 to 15 km from the drill sites, which are 50 thousand to 250 thousand years old (*11*). Also, Ba/Zr ratios are <1 and Ti/V ratios are ~20 in the rift basalts versus 1.5 to 2.5 and 10, respectively, in nearby Izu-Bonin arc basalts (*11, 14*). This difference precludes eruption of breccia components on the shallower arc. It also shows that basalt compositions lack arc-like geochemical characteristics even at the earliest stage of backarc basin development.

The matrix glass is approximately saturated in pure water for 2000 mbsl, but is undersaturated in pure CO_2 and S (Table 1). Similar data for nearby sea floor lava have been interpreted as indicating that the basalts were saturated with a mixed-volatile gas phase and had high pre-eruption H_2O/CO_2 and H_2O/S ratios (*11*).

Although the clasts are compositionally similar, their texture, paleomagnetism, and stable isotopes indicate that they have a separate history and probably are accidental. Texturally, the clasts are more crystalline and more devitrified than the glassy matrix (Fig. 3B) and thus cooled more slowly. Some clasts have chilled margins. Reaction zones between clasts and matrix suggest that the clasts were water-saturated when entrained. One clast has a low-temperature magnetic overprint, and the two that were separated from their surrounding matrix differ from it in paleoinclination. The H, C, and S isotope ratios of the clasts, and their relatively high C and SO_4 contents, indicate that they interacted at low temperature with seawater (Table 1). Whether the clasts represent sea floor scoria incorporated during eruption or xenoliths entrained from conduit walls is unknown. In any case, the clasts cooled separately and interacted more with seawater than did the matrix.

The texture and paleomagnetic characteristics of the matrix suggest that the unit is the product of an explosive eruption, the frothy pyroclasts of which welded within a steam envelope surrounding a small sea floor cinder cone. Explosive eruption is inferred because the breccia is fragmental at all scales (Fig. 3) and pillow lava fragments are absent. We interpret the domains in the matrix as spatter resulting from submarine fountaining of gas-rich magma. The domains differ from subaerial spatter because they vented at 20 MPa and chilled quickly. However, the absence of abundant shards with >70% vesicles may imply that magmatic volatiles were not the sole cause of explosivity (*15*), although the lack of such shards may also reflect the high-pressure eruption environment. Probably, the explosions were combinations of fountaining or Strombolian discharge on the one hand, plus contact-surface explosivity on the other. At a minimum, high pre-eruption gas contents contributed to the explosiveness by making the eruption more turbulent, and the high bubble content would have increased the surface area and viscosity.

The nature of the exsolved gas phase is poorly constrained by the available H-C-S data (Table 1). The high $H_2O/(CO_2 + S)$ ratio of the clasts and matrix is shared by glassy rims of the younger pillow lavas of the Sumisu Rift (*11*). These ratios are inferred to be pre-eruption features, so that the magmatic gas, even at 20 MPa, may have been rich in H_2O. The phenocryst compositions also imply that water pressure was high: the olivines are too Fe-rich and the plagioclases too Ca-rich for equilibrium with the bulk sample at 1 bar (*16*). A 25% porosity is equivalent to exsolving about 0.4% H_2O (by weight) at 20 MPa if ideal gas behavior at 1200°C is assumed. Differences between the highly vesicular pyroclasts in the Sumisu Rift and the nonvesicular hyaloclastites attributed to deep-water fire-fountaining at similar depths on intraplate seamounts (*17*) are related to higher magmatic water content in the backarc environment.

Three observations indicate that the matrix was assembled while hot despite accumulation in deep water. First, its texture is similar to that of subaerial agglutinate and appears welded (Fig. 3). Variations in the percent and deformation of vesicles occur in the matrix, but it is difficult to determine domain boundaries because of the welding. Second, the clasts show no evidence of mechanical abrasion, and there are no epiclastic interbeds in the 135-m-thick unit. Third, the high intensities, high temperatures, and stability of magnetic remanence in the matrix indicate hot deposition. Welding requires thermal isolation from surrounding seawater. Nevertheless, the vesicular sidero-

Table 1. Representative chemical analyses of breccia matrix and clast from ODP Core 791B. Analyses were obtained by x-ray fluorescence on the JOIDES *Resolution*; precision and accuracy are 1 to 5%; oxides are in weight percent; trace elements in parts per million. In addition, <10 ppm Ce and <30 ppm Ba are present; "Sum" is the total of the oxides in an ignited powder and does not include LOI (loss on ignition). The clast is sample 62R-1, piece 5; the matrix is sample 67R-1, piece 5. Concentrations and isotopic compositions of volatile elements were analyzed at Okayama University, Misasa, Japan (*11*); S and C were extracted with the use of the Ueda-Sakai method (*19*). Two samples each of bulk matrix and clast were analyzed for volatiles: clasts, 62R-1, 29 to 31 cm, and 62R-1, piece 5; matrix, 62R-1, 51 to 53 cm, and 67R-1, piece 5. Both samples for which results are tabulated above were analyzed for all elements. In addition, hand-picked glass from matrix sample 63R-1, 93 to 100 cm, was analyzed. It contained 1.35 weight percent H_2O with $\delta D = -53$. Isotopic ratios are expressed as per mil deviations from those in a standard.

Component	Clast	Matrix
SiO_2	48.59	49.76
TiO_2	0.96	1.04
Al_2O_3	16.99	17.58
Fe_2O_3	10.67	12.02
MnO	0.15	0.18
MgO	8.25	8.72
CaO	12.11	8.43
Na_2O	2.28	2.41
K_2O	0.15	0.54
P_2O_5	0.48	0.07
(LOI)	1.49	6.32
Sum	100.63	100.75
Rb	2	4.8
Sr	260	172
Zr	47	46
Nb	0.9	1.1
Y	29	16
Ni	43	52
Cr	186	181
V	353	355
Cu	55	54
H_2O*	1.15	2.24
δD (SMOW)	−70.7	−61.3
C (ppm)	220 to 328	19 to 10
$\delta^{13}C$ (PDB)	+0.2	
Sulfide (ppm)	6	28
$\delta^{34}S$ (CDT)	+11.0	+0.8 to 1.6
Sulfate (ppm)	38 to 88	+0.6 to 1.0
$\delta^{34}S$ (CDT)	+11.0 to 19.6	

*In weight percent

melane glass implies that rapid quenching occurred, perhaps within steam clouds above the vent on the sea floor.

A final surprising implication of the paleomagnetic results is that the cooling units of the breccia are at most a few meters thick. Paleoinclinations of the matrix are random between pieces of core rather than uniform as they should be had the deposit welded as a single cooling unit. If the samples had been uniformly magnetized upon deposition at 31°N during the Matuyama reversed epoch, then they all would be inclined $-50° \pm 5°$. Paleoinclinations are not expected to be affected by drilling rotation. In contrast, no two adjacent pieces of core have the same inclination, and many pieces are overturned. Inclinations of the matrix do agree within one 20-cm-long core and within five of seven minicores ($10\ cm^3$); these data indicate that samples at these scales belong to the same cooling unit. The maximum distance between adjacent randomly oriented cores is 2.5 m, so that cooling units are at least that thin.

The paleomagnetic heterogeneity shown by the matrix may have been caused by welding within the eruption column, or on the steep slopes of a small sea floor cinder cone. Welding may be more likely in a submarine than subaerial eruption column because dispersal is less rapid and fragments can be convectively reentrained while hot, even though they are quenched (*18*). In this interpretation, matrix domains acquired their remanent magnetism in the eruption column and landed randomly. Alternatively, rapid mass wasting of agglutinated cinders during the eruption could result in the random orientations encountered. In this interpretation, welding occurred during deposition on the sea floor and the randomness reflects subsequent slope instability. The absence of similar breccia at Site 790 only 2.4 km away is consistent with the inference of a small steep-sided edifice, but the available evidence is inconclusive about where welding occurred.

In summary, the matrix of this scoriaceous basaltic breccia suggests explosive eruption, hot deposition, and thin cooling units despite eruption at >18 MPa. The obvious clasts appear to be accidental. The occurrence in deep water of these phenomena, which usually are associated with subaerial eruptions, result from the high water content of backarc tholeiitic basalt magma. Although H_2O is much more soluble than CO_2 in magma and has a smaller work function at these pressures, the recycling of much more H_2O than CO_2 at subduction zones creates the potential for deep explosive eruptions. Terrestrially, the association of high magmatic water with eruption at confining pressures >18 MPa is characteristic of backarc basins.

REFERENCES AND NOTES

1. R. V. Fisher and H.-U. Schmincke, *Pyroclastic Rocks* (Springer-Verlag, Berlin, 1984).
2. J. G. Moore, *Nature* **282**, 250 (1979); ——— and J. G. Schilling, *Contr. Mineral. Petrol.* **41**, 105 (1973).
3. J. R. Delaney *et al.*, *Geochim. Cosmochim. Acta* **42**, 581 (1978); A. D. Saunders and J. Tarney, *ibid.* **43**, 555 (1979); H. J. B. Dick, *Initial Reports of the Deep-Sea Drilling Project* (U.S. Government Printing Office, Washington, DC, 1981), vol. 58, pp. 895–904; J. W. Hawkins and J. T. Melchior, *J. Geophys. Res.* **90**, 11,431 (1985); R. Poreda, *Earth Planet. Sci. Lett.* 73, 244 (1985).
4. R. Sparks, *J. Volcanol. Geotherm. Res.* **3**, 1 (1978).
5. K. H. Wohletz, *Bull. Volcanol.* **48**, 245 (1986).
6. P. Kokelaar, *ibid.*, p. 275.
7. ODP Leg 126 Shipboard Scientific Party, *Nature* **342**, 18 (1989).
8. E. Honza and K. Tamaki, in *The Ocean Basins and Margins*, A. E. M. Nairn *et al.*, Eds. (Wiley, New York, 1985), vol. 7A, pp. 459–502; B. Taylor *et al.*, *Earth Planet. Sci. Lett.*, in press.
9. The characteristic species include *Uvigerina hispidocostata, Oridorsalis umbonatus, Cibicidoides wellerstorfi, Stilostomella* spp., *Melonis barleeanus, Melonis pompilioides, Pullenia bulloides*, and *Pieurostomella* spp.; shallower fauna such as *Buliminia aculeata* are absent.
10. H. Yasuda, in *Collected Papers on Foraminifera from the Japanese Islands* (Toko Press, Sendai, Japan, 1989), pp. 83–92.
11. A. G. Hochstaedter *et al.*, *Earth Planet. Sci. Lett.*, in press.
12. Fo, forsterite component of olivine; An, anorthite component of plagioclase.
13. A. D. Saunders and J. Tarney, in *Marginal Basin Geology*, B. P. Kokelaar and M. F. Howells, Eds. (Blackwell, Oxford, 1984), pp. 59–76; J. M. Sinton and P. Fryer, *J. Geophys. Res.* **92**, 12,782 (1987).
14. Y. Zhang and C. Langmuir, personal communication.
15. B. F. Houghton and C. J. N. Wilson, *Bull. Volcanol.* **51**, 451 (1989).
16. Assumes that K_D $(FeO^*)/MgO_{ol} = 0.3$ and K_D $(An/Ab)_{plag} = 1.0$ indicate low-pressure anhydrous conditions, whereas higher K_D's indicate higher water pressures where K_D is a distribution coefficient, FeO^* is total iron, the Ab is the albite component of plagioclase, and ol is olivine; T. C. Juster, T. L. Grove, M. R. Perfit, *J. Geophys. Res.* **94**, 9251 (1989); M. G. Morrice and J. B. Gill, *J. Volcanol. Geotherm. Res.* **29**, 311 (1986).
17. T. L. Smith and R. Batiza, *Bull. Volcanol.* **51**, 96 (1989).
18. H. Staudigel, personal communication.
19. H. Kuno, *Cat. Active Volcan.* **9** (1962).
20. A. Ueda and H. Sakai, *Geochem. J.* **17**, 185 (1983).

21. This serendipitous, multi-disciplinary discovery was possible because of the Ocean Drilling Program. Shipboard chemical analyses, thin sections, and photographs were provided by ODP staff, especially B. Domeyer, K. Kuroki, and C. Galida. B. Houghton, H. Staudigel, and D. Clague provided helpful reviews.

7 February 1990; accepted 12 April 1990

A Comparison of the Contribution of Various Gases to the Greenhouse Effect

HENNING RODHE

The current concern about an anthropogenic impact on global climate has made it of interest to compare the potential effect of various human activities. A case in point is the comparison between the emission of greenhouse gases from the use of natural gas and that from other fossil fuels. This comparison requires an evaluation of the effect of methane emissions relative to that of carbon dioxide emissions. A rough analysis based on the use of currently accepted values shows that natural gas is preferable to other fossil fuels in consideration of the greenhouse effect as long as its leakage can be limited to 3 to 6 percent.

THE GREENHOUSE EFFECT OF A CERtain amount of a greenhouse gas in the atmosphere can be estimated with radiative transfer calculations. Even though considerable uncertainty is associated with calculations of an expected increase in temperature, the relative contribution of various gases can be determined more accurately (see Table 1).

The effect of 1 mol (or 1 kg) of CO_2 in the atmosphere depends to some extent on the prevailing concentration of CO_2. At present, high atmospheric concentrations of CO_2 already prevail and the effect of additional CO_2 is less. No corresponding saturation effect has yet occurred with the other greenhouse gases. The values in Table 1 are based on current CO_2 levels; consequently, future comparison values for the various gases will be somewhat greater.

When these relative values are scaled according to the currently observed increase in concentrations in the atmosphere, the relative contributions of the gases to the greenhouse effect are obtained (Table 2). The percentage contributions are uncertain because of uncertainties in both the values in Table 1 and the observed rate of increase. The latter uncertainty is particularly true for ozone (O_3) in the troposphere. The total effect is expected to cause an increase in the average global temperature of 1.5 to 4.5 K sometime around the middle of the 21st century (*1*). Although CO_2 is the least efficient gas on a per mole basis, it is responsi-

Department of Meteorology, Stockholm University, S-106 91 Stockholm, Sweden.